Secondary Microflows in Electrokinetic Transport with Hydrodynamic Slippage Effect

Kwang Seok Kim, Myung-Suk Chun*, Young Tae Byun and Deok Ha Woo

Sensor System Center, National Agenda Res. Div., Korea Institute of Science and Technology (KIST), Seongbuk-gu, Seoul 136-791, Republic of Korea, mschun@kist.re.kr

ABSTRACT

The secondary flow motion that is induced by curvature of microscale channel is thoroughly studied with simulation and experimental validation. The steady-state solution of the electroosmotic flow is achieved by applying the full Poisson-Boltzmann and the Navier-Stokes equations that are associated throughout the whole domain of the rectangular microchannel, made of either glass only or glass and polydimethylsiloxane. At the hydrophobic surface with curvature, the generalized Navier's slip boundary condition is applied. The particle streak velocimetry is performed by using an inverted epi-fluorescence microscope with tracer particle, which provides experimental verifications. We visualize the flow in a curved microchannel and compare the results with the simulation. Based on the agreements, it is concluded that our simulations exactly represent the curvature induced secondary flow, and are able to provide standard predictor for the relevant applications.

Keywords: microfluidic chip, secondary flow, electrokinetics, hydrodynamic slip, particle streak velocimetry

1 INTRODUCTION

Electro-osmotic flow (EOF) is one of the fundamental electrokinetic phenomena and is able to play an important role manipulatining flows in lab-on-chips (LOCs) devices. The electric field E that is externally imposed along the channel leads to the movement of an electrolyte solution against a stationary wall [1]. In addition, curved channel is frequently encountered in LOCs because it provides a convenient way for increasing the channel length per unit chip area.

The curvature induces the secondary flow. As shown in Fig. 1, when an external electric field is imposed between the inlet and outlet of the channel, same potential drop occurs over arc AB and arc A′B′. Thus, a stronger field is created on the inside edge of the channel wall, driving a faster EOF. Thus, the gap of the flow path between the inner and outer walls in a curved channel yields the pressure distribution in the spanwise direction and evokes the flow in the direction. In this way, the secondary flow is known to facilitate a mixing in microscale channel. Therefore, the behavior of EOF with curvature-induced secondary motion is worth being studied for improvements and optimum design of the devices.

This study addresses the numerical investigation of EOFs in curved microchannels of rectangular cross-section as well as the experimental validation by the microflow visualizing technique. The simulation results of the streamwise and spanwise velocities are reported to examine the unique behavior of secondary microflow in shallow and deep channels. Strengthened secondary flow results from increasing the electric double layer (EDL) thickness and the contribution of fluid inertia (i.e., electric field and curvature), providing a scaling relation with the slope [2,3]. Our framework is applicable to the dissimilar configurations of the channel wall taking unequal surface charge and fluid slippage with adopting hydrophilic glass and hydrophobic polydimethylsiloxane (PDMS), which has not been fully attempted.

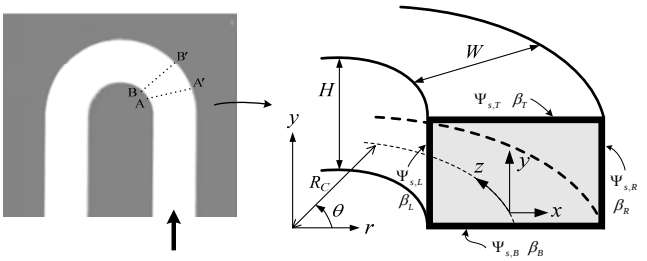

Figure 1: The curved channel with relevant coordinates system and each boundary condition.

2 MODEL FORMULATIONS

2.1 The Fluid Slip at Curved Wall

As shown in Fig. 1, the steady-state EOF through a curved microchannel of rectangluar cross-section (i.e., width W, height H, and curvature radius R_C) is considered. Fig. 1 also shows the coordinate transformation available between the global toroidal system and the Cartesian system, where r (= R_C + x) and y correspond to spanwise and longitudinal distances.

While no-slip boundary conditions (BCs) are applied to the wall of hydrophilic surface, the hydrodynamic BC at the hydrophobic surface undergoes the fluid slippage that is a function of the wettability indicated by the contact angle. At a uniform hydrophobic rigid boundary, fluid slippage at the stationary interface can be expressed by the so-called the

Navier's fluid slip condition [4,5] with a slip length (sometimes, Navier length) β such that

$$\boldsymbol{v}_t = \beta \boldsymbol{m} \cdot \left[\nabla \boldsymbol{v} + (\nabla \boldsymbol{v})^T \right]. \quad (1)$$

Here, β is a material parameter in length scale that is understood as the local equivalent distance below the solid surface at which the no-slip BC ($\beta = 0$) would be satisfied if the flow fields were linearly extrapolated out of the physical domain.

It is possible to derive the streamwise velocity by applying Eq. (1) to the curved region in Fig. 1, expressed as

$$v_\theta = \left(\frac{1}{\beta} + \frac{1}{R_C} \right)^{-1} \frac{\partial v_\theta}{\partial r} = \frac{\beta R_C}{(\beta + R_C)} \frac{\partial v_\theta}{\partial r}. \quad (2)$$

Then, $\beta R_C/(\beta + R_C)$ corresponds to the slip length β on a curved surface.

2.2 Electrokinetic Flow Equations

Once the non-conductive and non-neutral (charged) surface is in contact with an electrolyte in solution, the electrostatic charge would influence the distribution of nearby ions and the electric field is established [6]. For a uniformly charged rectangular channel, the nonlinear Poisson-Boltzmann (P-B) equation governs ψ such that

$$\nabla^2 \Psi = \kappa^2 \sinh \Psi. \quad (3)$$

Here, the dimensionless electric potential Ψ denotes $\Lambda e\psi/kT$ and the EDL thickness κ^{-1} is defined by $\kappa = (2n_b \Lambda_i^2 e^2/\varepsilon kT)^{1/2}$ with the valence of i ions Λ_i. Applying symmetric (Λ-Λ) electrolytes provides the same valences of cations and anions. The electrolyte ionic concentration in the bulk solution at the electroneutral state n_b (1/m^3) equals to the product of the Avogadro's number N_A (1/mol) and bulk electrolyte concentration (mM). The e is the elementary charge, and kT the Boltzmann thermal energy at room temperature.

The Dirichlet BCs of constant-potential surface are imposed on each side of the wall displayed in Fig. 1: $\Psi = \Psi_{s,L}$ at $x = -W/2$, $\Psi = \Psi_{s,R}$ at $x = W/2$, $\Psi = \Psi_{s,B}$ at $y = 0$, and $\Psi = \Psi_{s,T}$ at $y = H$. The subscripts stand for top (T), bottom (B), right (R), and left (L).

The steady state velocity $\boldsymbol{v}$ for an incompressible Newtonian fluid is combined with the continuity equation and Navier-Stokes (N-S) equation. The electric field can be given by the linear superposition of the external electric potential ϕ imposed by end-channel electrodes and the inherent electric potential ψ, providing that $\boldsymbol{E} = -\nabla(\phi + \psi)$. Originally, ϕ satisfies here the 2-dimensional Laplace equation (i.e., $\nabla^2 \phi(r,\theta) = 0$) in the outside region of the EDL. As the BCs, the Dirichlet conditions can normally be given at the inlet and outlet of the channel, and the Neumann conditions are assigned at the inside and outside walls of impermeable solid channel ($\partial \phi_{wall}/\partial r = 0$). It is acceptable that the spanwise dependence of ϕ is much smaller than its streamwise axial dependence, whereas the streamwise dependence of ψ is negligible. Then, streamwise electric field E_θ is defined by the external potential ϕ as $E_\theta = -\mathrm{d}\phi(\theta)/\mathrm{d}\theta$.

3 SIMULATION AND RESULTS

The well-established SIMPLE algorithm represented by the finite volume method (FVM) was employed in this study to solve the unknown pressure terms $p(x,y)$ of the momentum equation by using the continuity equation as the pressure-velocity coupling. The velocity and pressure corrections are accomplished by repeating the sequence of operations until the convergence is guaranteed. Note that the alternating direction implicit (ADI) method and staggered grid are adopted when the procedure comes to treat x and y components of discretized N-S equation and the continuity equation.

Computations are performed for the 1-1 type electrolyte of KCl fluid ($\rho = 10^3$ kg/m^3, $\mu = 10^{-3}$ Pa·s), where its EDL thickness κ^{-1} in nm is expressed as [fluid electrolyte concentration (M)]$^{-1/2}$/3.278. We consider two kinds of configurations with setting each side of channel walls as (I) glass (i.e., glass in all sides) and (II) glass in bottom and PDMS in the other sides, which are the most widely prepared and used in microchip electrophoresis. As the prototype of channel cross section, the dimension is set 25 μm wide and 5 μm deep for shallow geometry ($H/W = 0.2$, low-aspect-ratio) and 5 μm wide and 25 μm deep for deep geometry ($H/W = 5$, high-aspect-ratio), with the hydraulic radius R_h (= $HW/(H+W)$) of 4.17 μm. The values of the parameters used in the simulation is summarized in Table 1.

In the simulation, β of 100 nm is taken for partially non-wetting PDMS surfaces [9] (contact angle of ca. 98°) from the experiment that will be addressed later. We take here Ψ_s of PDMS as –0.78 (ψ_s = –20 mV), –1.56 (ψ_s = –40 mV), –2.33 (ψ_s = –60 mV), and Ψ_s of glass as –1.36 (ψ_s =

Table 1. Input parameters for the simulations.

Medium electrolyte (KCl) conc.	1–10^{-4} (mM) (i.e., κ^{-1} = 9.7–965 nm)
Dimensionless surface potential, Ψ	0.8–2.33 (PDMS) [7] 1.4–4.67 (glass) [8]
Slip length, β	100 nm (PDMS) No-slip (0 for glass)
$\Delta\phi$/L	50–300 (V/cm)
Viscosity, μ	10^{-3} Pa·s
Relative permittivity	78.9

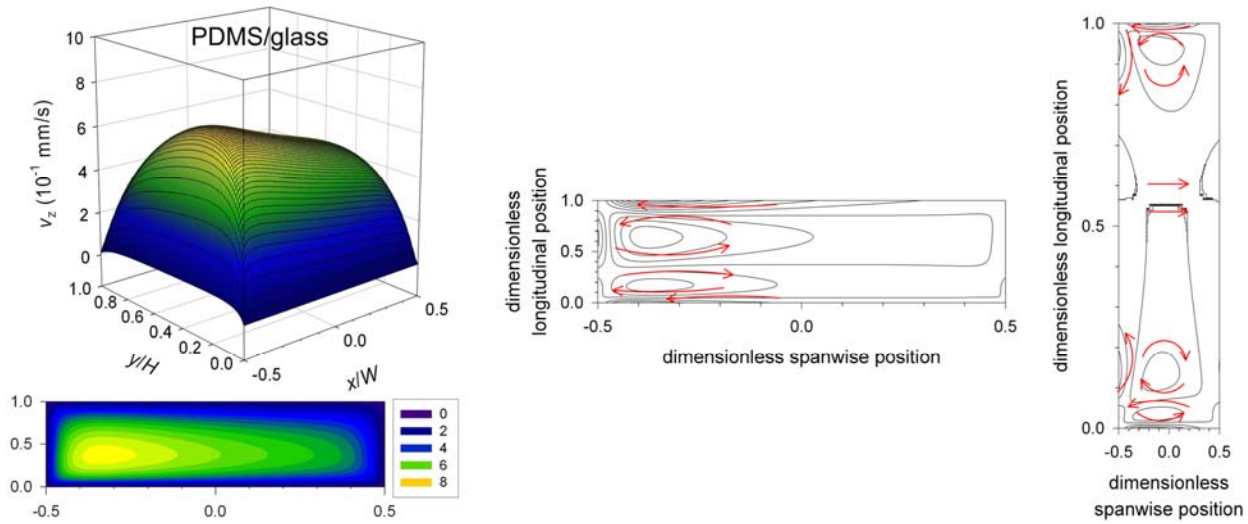

Figure 2: (Left) Streamwise velocity and its contour of shallow channel for thick EDL of 965 nm, (Right) vorticity contours of shallow (lying: H = 5 μm, W = 25 μm) and deep (standing: H = 25 μm, W = 5 μm) geometry, where PDMS/glass channels with W/R_C = 0.5, E = 100 V/cm.

–35 mV), –3.11 (ψ_s = –80 mV), –4.67 (ψ_s = –120 mV) for 1.0, 10^{-2}, and 10^{-4} mM KCl electrolyte, respectively.

Simulation results regarding the variations of spanwise velocities depending on electrokinetic parameters and fluid slippage show consistency with the predictions in the literature [10]. The graph on the right in Fig. 2 provides the streamwise velocity profile, corresponding to the EOF velocity. The magnitude of the streamwise velocity was found to be greater in the order of about 10^4 than that of the spanwise velocity. The Dean number of this study is estimated as very low values in the order of 10^{-2}~10^{-3}, from which the behavior of inward skewness is explained by a dominant effect of the spanwise pressure gradient over the fluid inertia by centrifugal force.

Secondary flows arise due to a mismatch of streamline velocity between fluid in the channel center and near-wall regions. The graphs on the right in Fig. 2 provides the vortices results in two channels with shallow and deep geometry, where the magnitude of difference between each contour line is all equal as 2×10^{-7} s^{-1}. The rotational direction is determined by a sign of the magnitude of vortex cell, with plus for anticlock-wise and minus for clock-wise. Evidently, the positions of maximum in the vorticity profile are located with shifting close to inner wall. A pair of counter-rotating vortices placed above and below the plane of symmetry of the channel is commonly found in the glass channel. On the contrary, PDMS/glass channel does not show this trend, but the close pattern appears to be developed near the bottom wall of the glass surface.

4 EXPERIMENTAL VALIDATION

The micro-particle streak velocimetry (μPSV) is performed by using an inverted epi-fluorescence microscope with tracer particle, which provides experimental verifications [11]. We first estimate the hydrodynamic slip length β on flat PDMS channel (H: 300 μm, W: 30 μm), and then conduct with curved PDMS microchannel (H: 25 μm, W: 5 μm, curvature radius = 5 μm) to validate the simulation results (see Fig. 2). To this end, we fabricate the microfluidic chip containing a curved PDMS microchannel by following the standard photolithography. An imaging system consists of an inverted epi-fluorescent microscope (Eclipse-Ti, NiKon, Japan), a fluorescent illuminator, and a digital charge-coupled device camera (NiKon, Digital Sight DS-Qi1, Japan) shown in Fig. 3. The 100 times magnification objective lens is used with an immersion oil. A focal plane is placed at 10 μm above the glass surface. A camera exposure time is set to 200 msec, and a frame rate is 30 fps. In a dark environment, images from the camera are recorded by the NIS-Elements software (NiKon, Japan).

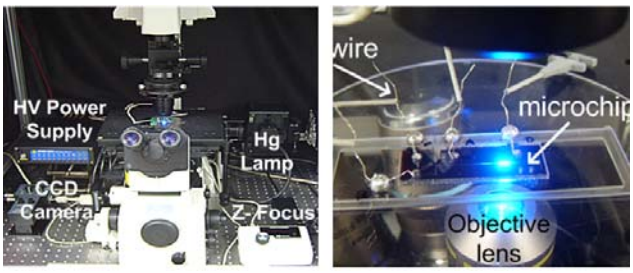

Figure 3: Experimental setup for μPSV flow visualization.

The test fluid is 10-ppm suspension of DI water and polystyrene latex beads of diameter 0.5 μm (L3280, Sigma Aldrich, MO). Beads are fluorescent red, exited by

wavelength of 575 nm, and emit 610 nm. Addition of 0.02 g Triton X-100 to every 100 ml suspension prevents beads from aggregation. A collection of streak images (Fig. 4) is processed by the MatLab algorithm that determines the local velocity in terms of a ratio of the real distance to the number of pixels.

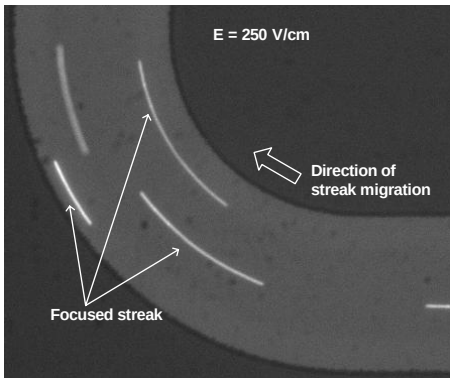

Figure 4: The streak images of the fluorescent bead taken during the camera exposure time (200 ms).

In Fig. 4, the streak images in the curve channel are obtained by using the charge coupled camera (CCD) mounted inverted epi-fluorescence microscope. The streamwise velocity is the length of an individual streak divided by the camera exposure time, which is set to 200 ms in this experiment.

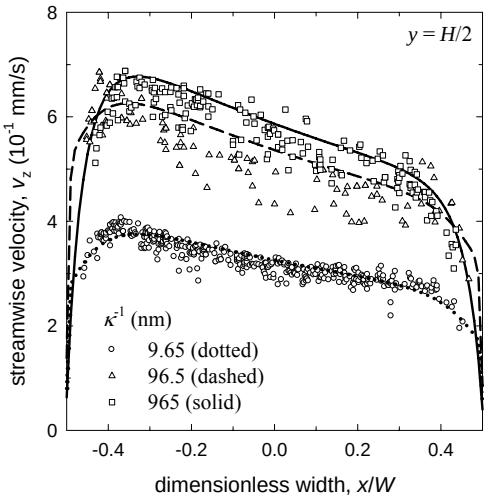

Figure 5: Streamwise velocity profiles obtained by simulations are compared with μPSV at various EDL thicknesses.

As a result, the streamwise velocities across the channel width are obtained both from simulations and the μPSV experiment, which show a fair agreement between them (see Fig. 5). Although the data are rarely obtained in the region near the channel walls, it can be found that thicker EDL drives the EOF faster, which has been expected by the simulations. Therefore, it is concluded that our simulations exactly represent the curvature induced secondary flow, and provide optimum selection in applications such as stronger secondary motion for mixing.

5 CONCLUSIONS

The curved channel is frequently encountered in the LOC system because it provides a convenient way for increasing the effective channel length per unit chip area. The behavior of steady EOF with secondary motion in curved microchannels was explored based on a model with P-B/N-S and the numerical framework developed by advanced scheme. Correct BCs of the hydrodynamic slip derived at curved surfaces were applied at each hydrophobic wall. Both the glass and the PDMS/glass channels were considered in the cases of shallow and deep geometry with taking the coupled effect of the EDL and the fluid slip for $\kappa\beta \cong 0.1\text{-}10$. Our simulation results regarding the variations of streamwise velocity according to κ^{-1}, ψ_s, and β were qualitatively matched with the analytical predictions reported in the literature, and the experimental result obtained by the μPSV.

ACKNOWLEDGMENTS

This work was supported by the Future-Oriented Research Fund (No. 2E23831) from the KIST and the Basic Research Fund (20100021979) through the National Research Foundation of Korea.

REFERENCES

[1] T.M. Squires and S.R. Quake, Rev. Mod. Phys. 77, 977, 2005.
[2] M.-S. Chun, Phys. Rev. E 83, 036312, 2011.
[3] J.-M. Lim, M.-S. Chun, Phys. Fluids 23, 102004, 2011.
[4] E. Lauga and H.A. Stone, J. Fluid Mech. 489, 55, 2003.
[5] D.P.J. Barz and P. Ehrhard, Lab Chip 5, 949, 2005.
[6] L. Bocquet and J.-L. Barrat, Soft Matter 3, 685, 2007.
[7] G.M. Mala, D. Li, C. Werner, H.-J. Jacobasch and Y.B. Ning, Int. J. Heat Fluid Flow 18, 489, 1997.
[8] J. Song, J.F.L. Duval, M.A.C. Stuart, H. Hillborg, U. Gunst, H.F. Arlinghaus and G.J. Vancso, Langmuir 23, 5430, 2007.
[9] P. Joseph and P. Tabeling, Phys. Rev. E 71, 035303R, 2005.
[10] L. Joly, C. Ybert, E. Trizac and L. Bocquet, J. Chem. Phys. 125, 204716, 2006.
[11] M.-S. Chun and S. Lee, Colloids Surf. A 267, 86, 2005.